UNIVERSITY of York

This is a repository copy of *Tunable Supramolecular Hydrogels for Selection of Lineage-Guiding Metabolites in Stem Cell Cultures*.

White Rose Research Online URL for this paper:
https://eprints.whiterose.ac.uk/id/eprint/153519/

Version: Accepted Version

Article:
Alakpa, Enateri V., Jayawarna, Vineetha, Lampel, Ayala et al. (15 more authors) (2016) Tunable Supramolecular Hydrogels for Selection of Lineage-Guiding Metabolites in Stem Cell Cultures. Chem. 298–319. ISSN: 2451-9308

https://doi.org/10.1016/j.chempr.2016.07.001

Reuse
Items deposited in White Rose Research Online are protected by copyright, with all rights reserved unless indicated otherwise. They may be downloaded and/or printed for private study, or other acts as permitted by national copyright laws. The publisher or other rights holders may allow further reproduction and re-use of the full text version. This is indicated by the licence information on the White Rose Research Online record for the item.

Takedown
If you consider content in White Rose Research Online to be in breach of UK law, please notify us by emailing eprints@whiterose.ac.uk including the URL of the record and the reason for the withdrawal request.

White Rose university consortium
Universities of Leeds, Sheffield & York

eprints@whiterose.ac.uk
https://eprints.whiterose.ac.uk/

Tuneable supramolecular hydrogels for selection of lineage guiding metabolites in stem cell cultures

Enateri V. Alakpa[1], Vineetha Jayawarna[2], Karl V. Burgess[3], Christopher C. West[4], Sanne C.J. Bakker[2], Sangita Roy[2], Nadeem Javid[2], Scott Fleming[2], Dimitris A. Lamprou[5], Jingli Yang[1], Angela Miller[1], Andrew J. Urquhart[5], Pim W.J.M. Frederix[2,6], Neil T. Hunt[6], Bruno Péault[4,7], Rein V. Ulijn[2,8*§] & Matthew J. Dalby[1*§]

[1] Centre for Cell Engineering. Institute of Molecular, Cell & Systems Biology, College of Medical, Veterinary & Life Sciences Joseph Black Building, University of Glasgow G12 8QQ, UK.

[2] WestCHEM, Department of Pure & Applied Chemistry, University of Strathclyde, 295 Cathedral Street, Glasgow G1 1XL, UK.

[3] Scottish Polyomics Facility. Wolfson Wohl Cancer Research Centre, College of Medical, Veterinary & Life Sciences, University of Glasgow, Garscube Estate, Glasgow G61 1QH, UK.

[4] Centre for Regenerative Medicine and Centre for Cardiovascular Science, University of Edinburgh, Edinburgh EH16 4UU, UK.

[5] Strathclyde Institute of Pharmacy and Biomedical Sciences (SIPBS), University of Strathclyde, Glasgow, UK.

[6] Department of Physics, University of Strathclyde, SUPA, Glasgow, UK

[7] Orthopaedic Surgery Dept and Broad Stem Cell Research Center, University of California, Los Angeles, USA.

[8]Advanced Science Research Center (ASRC) and Hunter College, City University of New York, NY 10031, USA.

Correspondence to matthew.dalby@glasgow.ac.uk or rein.ulijn@asrc.cuny.edu

§ co-senior authorship

Abstract.

Stem cells are known to differentiate in response to chemical and mechanical properties of the substrates that they are cultured on. As such, supramolecular biomaterials with tuneable properties are well-suited to study stem cell differentiation. In this report we demonstrate that metabolites can be identified that are selectively depleted during differentiation of perivascular stem cells on supramolecular peptide gels of different stiffness. On soft (2 kPa), stiff (15 kPa) and rigid (40 kPa)) we observe neuronal, chondrogenic and osteogenic differentiation. By analysing concentration variances of >600 metabolites during differentiation on the stiff and rigid gels (focusing on chondrogenesis and osteogenesis as regenerative targets) we identified that specific lipids, lysophosphatidic acid and cholesterol sulphate respectively are significantly depleted. We propose that these metabolites are therefore involved in the differentiation process. We subsequently demonstrate that these individual lipids can, when fed to standard stem cell cultures, induce differentiation towards chondrocyte and osteoblast phenotypes. Our concept exploits designed supramolecular biomaterials design as a new strategy for discovery of cell directing bioactive metabolites of therapeutic relevance.

Bigger Picture.

Adult stem cells, such as mesenchymal stem cells and perivascular stem cells (pericytes) represent autologous cell types that are excellent candidates for regenerative medicine. Controlling the differentiation of these stem cells with drugs, including small molecules, is highly desirable to elicit targeted regeneration. However, identification of these stem cell inducing molecules is non-trivial and rational approaches to discover drugs for achieving reproducible, targeted stem cell control remain elusive. Here, we demonstrate the design of supramolecular hydrogels that allow targeting of a range of stem cell phenotypes, providing a useful platform for discovery of differentiation inducing metabolites. These gels are simple in composition, containing a fibre forming aromatic peptide amphiphile, which is co-assembled with a surfactant-like amphiphile that provides hydrophilic surface functionality to the fibres. The stiffness of the gels can be precisely tuned over the entire range that is typically associated with stem cell differentiation (0.1-40 kPa).

We demonstrate that the gels can be used to direct stem cell differentiation without the need for induction media and they are therefore ideally suited to study stem cell behaviour –including as drug discovery platforms. To achieve this, we study the cell's usage of biological small molecules, metabolites, during differentiation and select bioactive metabolites that can target bone and cartilage formation specifically. This new use of designed supramolecular biomaterials can be envisaged to remove serendipity from discovery of metabolites associated with biological processes as drug candidates.

eTOC Blurb.

To facilitate metabolomics analysis of stem cell differentiation, supramolecular hydrogels were designed with tuneable stiffness but simple chemical functionality. These novel gels facilitate stiffness-tuned stem cell differentiation and could be used to survey the usage of biological small molecules during differentiation, with potential as drug candidates. We thus identify candidate bioactives targeting bone and cartilage formation from perivascular and mesenchymal stem cells opening the potential new area of using supramolecular biomaterials as a platform for drug discovery.

Introduction.

As stem cells differentiate in response to their physical and (bio-)chemical environment, divergent metabolomic activities and alterations in energy demand occur. It is likely that stem cells control their metabolome to help prevent spontaneous differentiation[1-3]. Then, as they differentiate, metabolism alters and diverges as the cells 'activate'[1-4]. As such, the metabolic activity of the cells may be expected to contain specific metabolite depletion patterns that are linked to differentiation. If these metabolites can be identified, it may be possible to induce differentiation by 'feeding' these molecules to stem cell cultures.

Metabolites are of increasing interest in control of cell function and differentiation and addition of metabolites to cultures has been shown to *e.g.* promote monocyte to iron-recycling macrophage commitment[5]. Less, however, is known about key

regenerative cell types such as stem cells and the identification of metabolites that influence specific cell behaviour is currently challenging.

We theorised that we could use a conceptually new approach, a strategy that firstly uses supramolecular biomaterials[6-9] to create environments that mimic aspects of the extracellular matrix and differentially induce stem cell differentiation, and secondly, by using these gels to observe and compare metabolite depletion during stem cell differentiation in these gels and finally to test whether bioactive metabolites that are uniquely depleted during these differentiation experiments in turn control stem cell differentiation in standard cultures. This approach would provide a new use of designed supramolecular biomaterials as a platform to accelerate discovery of metabolites as drug candidates.

Using a physical (designed cell environment), rather than the more conventional biochemical (use of growth factors), approach to trigger differentiation is ideally suited to metabolomics experiments as it avoids changing media formulations to control growth and differentiation and thus allows for a direct comparison when targeting different lineages. Indeed, changing media recipes could add significant artefact to metabolite analysis.

Several types of physical and chemical cues have been shown to influence mesenchymal stem cell (MSC) growth[3, 10-12] and differentiation[13-17] involving especially alterations in surface chemistry, topography and stiffness. In particular for ability to target a range of MSC fates, tissue matching of stiffness is of considerable interest[12, 13, 18-22]. MSCs cultured on soft, neural tissue-like, matrices (~2 kPa) show a tendency to differentiate toward cells expressing neural markers, when they are cultured on surfaces with similar elastic properties to muscle (~10 kPa) they form myocytes and when cultured on rigid substrates, mimicking pre-calcified bone (~40 kPa), MSCs become osteoblasts[13].

For the purpose of our work, we seek to control stiffness over a physiological range of storage moduli while keeping molecular structures as simple as possible, as even

small chemical changes can produce substantial effects in cellular response[23]. We have therefore developed hydrogels composed of fibers with simple cytocompatible surface functionality[24] and tuneable network densities. The gels are well suited to cell culture as they are prepared from free-flowing precursor solutions which gelate upon exposure to calcium ions present in culture media. The materials ideally fit with our desire to keep the cell growth conditions as chemically identical as possible so as not to bias the metabolomics experiments.

Thus, we firstly set out to develop simple stiffness-matched gels that are able to drive stem cell differentiation. We then use data mining from global metabolomics experiments to allow identification of endogenous, individual, bioactive metabolites. We specifically look for bioactive metabolites that are depleted when comparing differentiation in different gels. Finally, thus identified metabolites are fed to stem cell cultures to assess their ability to control and direct differentiation.

Results.

Formulation and characterisation of varying stiffness gels with minimal chemical differences.

The first objective was to produce chemically similar, cytocompatible hydrogels with varying stiffness in the physiologically relevant range to enable step 1, use tissue-matched gels to drive stem cell differentiation.

Hydrogels are well suited for the production of cell-matched environments. Stiffness control of polymeric hydrogels is typically achieved using differential chemical crosslinking[13, 14]. Supramolecular hydrogels[7,8, 25,26,27], however, provide an alternative approach where stiffness and chemical composition can be systematically varied. Most gels studied to date include bioactive groups, typically introduced through coating of the substrate with extracellular matrix components or by chemical functionalization with bioactive groups (*e.g.* proteins or peptide motifs)[28-30]

In order to tailor suitable materials, we made use of a two-component co-assembly approach comprising a peptide based gelator (the structural element) and a

surfactant-like molecule that presents carboxylate functionality to the surface of fibres[31], enabling subsequent cross-linking upon exposure to divalent cations (Ca^{2+}) present in tissue culture media. Specifically, when fluorenyl-9-methoxycarbonyl-diphenylalanine, Fmoc-F_2[24, 32, 33] was co-assembled with surfactant-like Fmoc-serine (Fmoc-S), the polar serine side chains were presented at the surface of the fibres (Fig 1a). The differential organisation of the gelator and surfactant components in isolation is evident from atomic force microscopy images (Fig 1b) and static light scattering (Supplemental Fig 1a), with nanofibres and spherical aggregates observed, which upon mixing co-assemble as fibres. The mode of self-assembly is further supported by fluorescence spectroscopy (Fig 1c) and Fourier transform infrared spectroscopy (FTIR) (Fig 1d).

Formation of hydrogels with tuneable stiffness was achieved by varying co-assembly concentrations giving rise to viscous liquids in the concentration range 5-40 mM. The presence of carboxylate ions at the fibre surface allows for these structures to be stabilised and subsequently physically crosslinked by exposure to tissue culture media. Gradual exposure to the media is achieved by diffusion through semipermeable membrane of cell culture inserts, resulting in gelation within approximately 90 minutes.

Oscillatory rheology of the resulting gels revealed elastic moduli of 0.1 kPa up to 40 kPa with increasing concentration (Fig 1e). In each case, the elastic modulus G' exceeded the viscous modulus G", indicating that these gels are predominantly elastic in nature (Supplemental Fig 1c). The results show that variation of the concentration of fibres can result in gels with moduli close to values reported for neural, muscle and bone-like tissues[34]. Note that stiffness values in the literature are obtained using various testing methods, and either Young's or storage moduli are reported[25]. Visual examination (Fig 1f) of the gel samples reveals a clear correlation in the appearance with the network properties (Supplemental Fig 1d).

FTIR spectroscopy of the gels in D_2O solution with salt composition identical to that present in culture media (for composition, see methods)[35] revealed significant

differences in the hydrogen bonding arrangements in pre-gelation mixtures and gels with peak broadening observed with increasing concentrations (Supplemental Fig 1 e&f). The broadening peak around 1590 cm^{-1} (COO^- stretch) indicates that at least a proportion of the C-termini are deprotonated. As expected, the intensities of amide I bands increase with concentration as fibre density increases and is more pronounced in the gels compared to the starting mixtures. Fluorescence emission spectra of the pre-gelation mixtures at increasing concentrations show quenching of the monomeric emission (Supplemental Fig 1 g&h) where the excimeric emission becomes more pronounced. These results are in agreement with increased fibre densities (fibre size, density and roughness and shown in Supplemental Fig 1 i&j). Cell attachment to the fibres likely involves absorption of serum proteins from cell culture media. Supplemental Fig 2k shows quenching of Fmoc fluorescence in the presence of fibronectin, vitronectin and total serum suggesting that the proteins interact with the fibres as fluorenyl emission is quenched in the presence of matrix proteins. In the remainder of this report, we use gels at 10, 30 and 40 $mmol.L^{-1}$, denoted as 2 kPa 'soft', 15 kPa 'stiff' and 40 kPa 'rigid'.

Analysis of primary pericyte differentiations.

In this study we use both MSCs and perivascular stem cells (pericytes) to demonstrate the generality of our approach. While MSCs hold great regenerative potential, autologous cells are available from *e.g.* iliac crest aspiration in vanishingly small numbers. Pericytes are the multipotent progenitors of MSCs and are readily available in large numbers from adipose tissue harvested by liposuction[36]. This availability, plus the ability to precisely characterise them, makes them an excellent autologous multipotent cell source able to differentiate into cells of the reticular, adipose, cartilaginous and bony lineages[36].

Multipotent pericytes (Supplemental Fig 2) cultured on the hydrogel surfaces and glass controls were assessed for primary differentiation lineages after 1 week of culture using quantitative (q)PCR. These were ascertained as neurogenesis, chondrogenesis and osteogenesis respectively through the increased production of the markers β3 tubulin (neural protein), SOX9 (sex determining region Y-box 9, chondrogenic directing transcription factor) and RUNX2 (runt related transcription

factor 2, osteogenic directing transcription factor) (Fig 1g-i, confirmatory data for additional neurogenic, myogenic, adiopogenic chondrogenic and osteogenic markers shown in Supplemental Fig 3). These data fit well within the established paradigm of stiffness directed MSC differentiation with soft gels inducing neural marker expression and rigid gels inducing osteogenesis[13, 34]. At 15 kPa we note expression of chondrogenic markers rather than myogenic (myoD, myogenic differentiation factor 1, a myogenic transcription factor was undetectable by PCR) previously reported in the 10 kPa range. This is perhaps because 15 kPa is closer to the stiffness of chondrons in which articular chondrocytes reside[37] or it may simply be due to differences between gel systems used.

Identification of candidate biological molecules.

Going forwards to identification of candidate biological molecules, we decided to focus on chondrogenesis and osteogenesis as key phenotypes classically targeted in regenerative medicine and tissue engineering (cartilage/bone repair). The intracellular complement of metabolites for cells cultured on each hydrogel surface were analysed after 1 and 4 weeks in culture. Liquid chromatography–mass spectrometry (LC-MS) analysis of the cell extracts permitted identification of individual metabolites of a total of 630-831 putatively identified metabolites. Observed changes largely fitted into four classes, amino acid, lipid, carbohydrate and nucleotide metabolism (Supplemental Fig 4). Lipids were chosen to focus on as this classification tended to show a depletion based profile on the substrates while amino acids, carbohydrates and nucleotides tended to become more abundant (Supplemental Fig 4). Lipid metabolite heatmap profiles showed a number of temporal (2 to 4 week) depletions were occurring. Metabolites were selected using the following criteria: (a) consider metabolites that were uniquely depleted upon culturing in one of the two stiffness hydrogels and (b) further select by choosing from these candidates metabolites that were unique to KEGG (Kyoto encyclopaedia of genes and genomes) pathways, *i.e.* we would not select chondro- and osteogenesis candidates from the same KEGG pathway in order to target distinct biosynthetic pathways. Using this methodology, a lysophosphatidic acid (1-octadecanoyl-sn-glycero-3-phosphate, GP18:0) belonging to the glycerolipid

pathway and cholesterol sulphate belonging to the steroid biosynthesis pathway were selected (Fig 2). We note that there are likely to be other interesting candidates in the pool of metabolites assessed. All lipid changes are shown in Supplemental Figs 5&6 and the full data set of depletion patterns is available (see materials and methods for DOI link).

Having identified these two metabolites, we considered their likely relevance in known cell type-specific processes. Lysophosphatidic acids (LPAs) such as GP18:0 can act *via* membrane bound G-protein coupled receptors and have been shown to regulate the mitogen activated protein kinases (MAPKs), more specifically extracellular signal-regulated kinase (ERK) pathways that are central in cell growth and differentiation[38]. Further, there is emerging evidence that murine cartilaginous bone mesenchymal cells express LPA receptors and that LPAs can have effects on chondroprogenitor activation as seen in the ATDC5 cell line[39] and in primary murine chondrocytes[40].

Cholesterol sulphate (CS) is a sterol lipid that resides primarily within the cell membrane providing structural support. However, CS in its own right can act as a regulatory molecule[41, 42]. Of the selected metabolites, CS was our only candidate that fitted into networks generated in Ingenuity pathway analysis® (IPA). On the rigid hydrogel, the analysis of metabolite pathways to layer metabolic information with known connections to biochemical pathways from pericytes reveals that CS may be used in transforming growth factor beta (TGFβ) signalling as it becomes depleted in pericytes (Supplemental Fig 7). The pathway analysis further implicates bone morphogenic protein signalling (BMPs are part of the TGFβ superfamily) - key to RUNX2 activation and hence osteogenesis[43] and implies ERK, ROCK, integrin (adhesion) and actin (cytoskeleton) signalling, tying in well to literature on osteogenesis[3, 13, 16, 17].

Testing biological molecule defined differentiation efficacy.

Having identified small molecules that potentially have roles in stem cell differentiation, we moved on to test their ability to direct differentiation. Due to the

expected central role in metabolic pathways we studied effects on both MSCs and pericytes. Testing of differentiation potential with serial dilutions (Supplemental Fig 8) revealed concentrations where effects on transcript expression were maximal.

To test osteogenesis and chondrogenesis, both pericytes and MSCs were cultured with 1 μM CS and 0.1 μm GP 18:0 in basic media (10% FCS/DMEM) on glass coverslips. For testing of osteogenic potential, cells were seeded as standard suspension cultures within the full volume of media and allowed to settle and adhere across the coverslip surface. For chondrogenic testing, cells were seeded in micromass cultures with all the cells being placed on the surface in a small, 20 μl, droplet of media and being allowed to attach and before flooding the wells with media. Micromass culture allowed us to establish conditions that enable, rather than drive, chondrogenesis and so suitably test our candidate metabolite.

Considering osteogenesis first, for cells seeded on to coverslips with CS added, expression of the mature bone-specific proteins osteocalcin and osteopontin were noted at similar levels to those observed in osteoinductive media for both pericytes (Fig 3a) and MSCs (Fig 3c) compared to negligible expression in controls. For pericytes and MSCs, measured expression of osteopontin was greater than un-stimulated control and similar to use of osteoinductive media (Figs 3b & d). Measurement of aggregated osteocalcin rich nodules revealed that mean nodule area was larger for pericytes treated with CS than osteoinductive media (Figure 3b) and it is noteworthy that no nodules were detected on untreated (no metabolite added) control. Image analysis of percentage of pericytes associated with osteocalcin rich nodules were 15.0±7.4% and 8.9±7.9% for CS and osteoinductive media respectively (no difference, $p=0.1$) compared to 0% for control ($p<0.05$). This illustrates comparable osteogenic differentiation between CS and osteoinductive media. Use of alizarin red staining for calcium in bone mineral (apatite, a calcium phosphate) also showed formation of nascent nodules when MSCs were treated with CS (Fig 3d). This was confirmed at transcript level with pericytes using primers for osteopontin and osteocalcin (Supplemental Fig 9a).

For pericytes and MSCs seeded (as micromass cultures) onto glass coverslips with GP18:0 added, similar expression of the cartilaginous proteins collagen II and aggrecan were noted to that of induction with chondrogenic media (Fig 3 e-g) and for MSCs, SOX9 expression was also shown to be enhanced (Fig 3h). This was confirmed at transcript level with pericytes using primers for collagen II and aggrecan (Supplemental Fig 9b).

Illustration of regenerative potential of bioactive metabolites.

Bioactive metabolites, such as those identified herein, could be drug candidates that influence metabolic pathways. We focus on CS as the candidate that fitted to well known canonical pathways in IPA® (likely because information on metabolite interactions is only emerging). As described, pathway analysis implicates CS with BMP signalling (Fig 5a, supplemental Fig 7). We hypothesise that CS could potentially be used as a much simpler alternative to BMP2 (the clinical standard) to provide enhanced osteogenesis. BMP2 signalling occurs through activation of the SMAD (SMA small body size and MAD mothers against decapentaplegic) pathway. Comparison of active (phosphorylated) SMAD 1 and 5 normalised to total SMAD 1 and 5 shows activation of the pathway with addition of CS (Fig 5b). Further, if BMP signalling is antagonised with noggin then CS fails to stimulate osteogenesis (Fig 5b).

To test effect of CS in a 3D tissue mimic in order to more closely resemble the *in vivo* situation, we formed a collagen gel and injected into it pericytes within the 40 kPa hydrogel with and without CS and cultured for 28 days (illustrated in Fig 5c). After culture without CS, three out of five tissue mimics were positive for extensive mineralisation as shown by von Kossa stain for phosphate. However, with CS, all five gels supported mineralisation and typically to a greater extent than using gel guidance alone (Fig 5c); this illustrates the potential ability of CS to mediate robust osseointegration in 3D. Such strategies could be important where ossification of soft tissues would be desirable, *e.g.* ossification of the masseter muscle in maxillofacial reconstruction of the jaw.

Discussion.

In these experiments we have shown that the use of metabolomics analysis coupled to simple tissue stiffness matched supramolecular hydrogels can be used to exploit stem cells' environmental adaptation processes for identification of novel bioactive metabolites that can define stem cell fate. Furthermore, individual bioactive metabolites were demonstrated to have similar efficiency to the complex cocktails of soluble factors currently used (e.g. dexamethasone with glycerophosphate and ascorbate for osteogenesis or dexamethasone, insulin and TGF-β1 for chondrogenesis) at a fraction of the cost.

We have discussed the potential for CS as an osteoinductive drug due to its better-known pathway. However, we note that GP18:0 may also have potential clinical use such as in matrix assisted autologous chondrocyte implantation (MACI) and has been developed for repair of osteoarthritic defects[44].

To conclude, this study demonstrates new methodology that uses designed supramolecular gels to allow for the facile identification of biological molecules that could be used to unlock the regenerative potential of stem cells. For the first time, the natural adaptation of stem cells to their physical environment was used to guide us to bioactive metabolite drug candidates. Peptide gels with simple composition and tuneable physical properties were developed specifically for stem cells to facilitate targeted differentiation and pericytes and MSCs were used as potential autologous stem cell sources. Into the future, this new approach could find further use in personalised medicine. In this scenario, a patient's stem cells would be analysed using biomaterials for bioactive metabolites during differentiation of the fate desired clinically. Thus, highly effective bioactives could be identified for optimal regeneration of that patient.

Experimental Procedures.

Materials

Fmoc-Serine (Fmoc-S) was purchased from Bachem Ltd., UK, with purity > 99.5%. Cell culture inserts for 12-well and 24 well multiwell plates with 1.0 µm pore size were purchased from Greiner bio-one, UK.

Synthesis of Fmoc-F_2

To a stirred solution of Fmoc protected L-Phenylalanine (1 equivalent) in dimethylformamide (DMF), coupling agent N,N,N',N'-Tetramethyl-O-(1Hbenzotriazol-1-yl)uronium hexafluorophosphate (HBTU) (1.2 equivalents) was added and stirred for 15 minutes. Then, hydrochloride salt of the C-terminal protected tert-butyl ester of L-Phenylalanine (1.2 equivalents) was added to the reaction mixture followed by addition of an organic base, diisopropylethyl amine (2.5 equivalents). Then the coupling reaction was allowed to stir for overnight. Solvent was evaporated out and the reaction mixture was dissolved in ethyl acetate. The ethyl acetate layer was washed with 1N sodium bicarbonate solution as well as 1N hydrochloric acid solution to remove any excess acid or base, followed by saturated brine solution. The organic layer was dried over magnesium sulphate and the solvent was evaporated. The final products were purified by column chromatography using 230-400 mesh silica gel as stationary phase and chloroform–methanol mixture as eluent.

Then, deprotection of the tert-butyl group is carried out in 50:50 mixtures of dichloromethane (DCM) and trifluoroacetic acid (TFA) for overnight. Then excess TFA is removed followed by the crystallization of the product from ether. Final traces of TFA were removed by continuous washing with ether. Powder analysed by using HPLC and it shows more than 98% purity.

Formation of the Fmoc hydrogels

Samples were prepared by mixing Fmoc-F_2 and Fmoc-S (Fmoc-F_2/S) (1:1 ratio) in 10 mL glass vials and suspending the powders to a specific peptide concentration in sterile/distilled H_2O. 0.5 M NaOH was added dropwise until the powders were fully

dissolved. The vial was mixed with alternated vortexing and sonication and then 0.5 M HCl was added until the desired pH was reached (7.5-7.8). Prior to use Fmoc-F_2/S pre gelation mixtures were sterilized under UV light for 45 min.

To produce hydrogels from each of these pre-gelation mixtures, 300 µL were transferred to cell culture inserts in 12-well plates. A volume of 1400 µL of culture medium was added to each well (outside the insert) and incubated for 1 ½ hrs at 37 °C in a humidified atmosphere with 5% CO_2. Following gelation the medium surrounding the inserts was replaced and 300 µL of new medium was gently added to the surface of the gels. Following overnight incubation the pH of the gel stabilized at around pH 7.8 (±0.5).

Fluorescence spectroscopy

Fluorescence emission spectra were measured on a Jasco FP-6500 spectrofluorometer with light measured orthogonally to the excitation light, with excitation at 280 nm and emission data range between 300 and 600 nm. The spectra were measured with a bandwidth of 3 nm with a medium response and a 1 nm data pitch. Experimental data were acquired in triplicate.

Fourier transform infrared spectroscopy (FTIR)

FTIR spectra were acquired in a Bruker Vertex spectrometer with a spectral resolution of 2 cm^{-1} and averaging 56 interferograms for each measurement. Gels were made in salt solution (DMEM, containing salts, for example, calcium chloride: 200mg/L; potassium chloride: 400 mg/L; sodium chloride: 6800 mg/L; magnesium sulfate: 97.7 mg/L; di-sodium hydrogen phosphate: 140 mg/L; sodium bicarbonate: 850 mg/L), made in D_2O. The samples were transferred into a standard IR cell holder (Harrick Scientific) and contained between two CaF_2 windows (thickness 2 mm) separated by a 25 µm PTFE spacer. D_2O (99.9 atom % D, Aldrich) was used as the solvent for all the IR measurements.

Rheology

To assess the mechanical properties of the hydrogels, dynamic frequency sweep experiments were carried out on a strain-controlled rheometer (Kinexus rotational

rheometer from Malvern) using a parallel-plate geometry (20 mm) with a 0.50 mm gap. An integrated temperature controller was used to maintain the temperature of the sample stage at 25°C. Precautions were taken to minimize solvent evaporation and to keep the sample hydrated: a solvent trap was used and the atmosphere within was kept saturated. To ensure the measurements were made in the linear viscoelastic regime, an amplitude sweep was performed and the results showed no variation in elastic modulus (G') and viscous modulus (G") up to a strain of 1%. The dynamic modulus of the hydrogel was measured as a frequency function, where the frequency sweeps were carried out between 1 and 100 Hz. The measurements were repeated at least three times to ensure reproducibility.

Atomic force microscopy (AFM)

For analysis of pre-gelation mixtures, 100 µL of mixture, prepared using the standard procedure described above, was placed on a trimmed, freshly cleaved mica sheet attached to an AFM support stub for 1 min. Upon removing any excess mixture by capillary action, the surface was rinsed twice with 200 µL of distilled H_2O and left to air-dry overnight in a dust-free environment, prior to imaging. To image the hydrogel structure, media is removed and gels were placed on mica sheet for 1 min and rinsed twice with 200 µL of distilled H_2O. The images were obtained by scanning the mica surface in air under ambient conditions using a Veeco MultiMode with NanoScope IIID Controller Scanning Probe Microscope (Digital Instruments, Santa Barbara, CA, USA; Veeco software Version 6.14r1) operated in tapping mode. The AFM measurements were obtained using a sharp silicon probe (TESP; nominal length (l_{nom}) = 125 µm, width (w_{nom}) = 40 µm, tip radius (R_{nom}) = 8 nm, resonant frequency (υ_{nom}) = 320 kHz, spring constant (k_{nom}) = 42 N m^{-1}; Veeco Instruments SAS, Dourdan, France), and AFM scans were taken at 512 x 512 pixels resolution. Typical scanning parameters were as follows: tapping frequency 308 kHz, integral and proportional gains 0.3 and 0.5, respectively, set point 0.5 – 0.8 V and scanning speed 1.0 Hz. The images were analyzed using Veeco Image Analysis software Version 6.14r1.

Transmission electron microscopy (TEM)

Carbon-coated copper grids (No. 400) were glow discharged for 5 s and placed shiny side down on the surface of the pre gelation mixtures and hydrogels for less than 5 s. Excess sample was removed by blotting with a filter paper and then 10 mL of negative stain (Nanovan: 1% aqueous methylamine vanadate, obtained from Nanoprobes) was placed on the top of the sample on the grid and allowed to dry for 10 mins. The dried specimens were then imaged using a LEO 912 energy filtering transmission electron microscope operating at 120 kV fitted with a 14 bit/2 K Proscan CCD camera. Fiber diameters were measured using ImageJ software version v1.43u.

Static light scattering (SLS)

Static light scattering measurements for pre-gelation mixtures were performed on 3DDLS instrument (LS instruments, Fribourg, Switzerland) using vertically polarized He-Ne laser light (25 mW with wavelength of 632.8 nm) with an avalanche photodiode detector at angles between 15° and 135° at 25 °C. The scattering intensity patterns from static light scattering experiments were analyzed by applying Guinier's law to calculate the shape-independent size parameter, radius of gyration (R_g).

In the range of Q-values higher than Guinier's region the scattering intensity can be described by power law:

$$I(Q) \propto Q^{-d_f}$$

Where, Q is the scattering vector amplitude ($Q = (4\pi n/\lambda)\sin(\vartheta/2)$, n is the refractive index of the solvent and λ is the wavelength of the laser). At intermediate Q, the exponent d_f reflects the dimensionality of the scattering object which is for instance, 1 for thin rod like particles.

Interaction of Fmoc F_2/S with fibronectin, vitronectin and serum proteins

The interactions of Fmoc-F_2/S fibers with different proteins fibronectin, vitronectin and serum protein in the concentration range relevant to cell culture conditions were characterized by Fluorescence based method as described previously[45]. The different concentrations of proteins were mixed with pre-gelation mixtures of Fmoc-

F_2/S and the quenching in emission fluorescence intensity was measured and the results are shown in Figures. The binding constants were calculated by applying the model described previously[45, 46].

Pericyte isolation

Pericytes were isolated from the adipose tissue of healthy adult donors undergoing cosmetic lipectomy procedures with prior written consent. Ethical approval for the collection of tissue and subsequent research was granted by the South East Scotland Research Ethics Committee 3 (SESREC03), reference number 10/S1103/45. Cells were purified to homogeneity by Flow Activated Cell Sorting (FACS) using a FACS Aria II (BD Biosciences) based on our established protocols[47]. Briefly, adipose tissue was enzymatically digested with type II collagenase (1mg/ml, Sigma-Aldrich) for 30 mins in a shaking waterbath at 37°C to obtain the Stromal Vascular Fraction (SVF). SVF was then stained with the following antibodies; CD146-Alexa647 (1:100, AbD Serotec, Raleigh, NC), CD45 APC-cy7, CD31-FITC, and CD34-PE (1:100, all from BD Biosciences, San Jose, CA). Pericytes were sorted to homogeneity based on the following phenotype CD146+, CD45-, CD34- and CD31-. Immediately following FACS, pericytes were seeded onto 0.1% gelatin coated wells at a density of 20,000 cells/cm2 in EGM-2 media (Lonza) in a humidified incubator with 5% CO2 at 37°C. When confluent, cells were detached from the cultureware using 0.25% trypsin and split at a ratio of 1:6 into uncoated wells and cultured in DMEM+20% FCS for all subsequent passages. Media was changed 3 times per week. Purity of pericyte cultures was confirmed by flow cytometry.

Cell Culture and Reagents

For cell culture, after overnight incubation of the hydrogel at 37°C, the basic, or standard, culture media (DMEM (PAA Laboratories) supplemented with 10% v/v foetal bovine serum (FBS) and 2% v/v antibiotic mix (60% v/v L-Glutamine, 35% v/v penicillin streptomysin and 5% v/v Ampotericin B)) on the surface and around the 12 well insert was removed. The media in the well was replaced with fresh media. The media on the surface of the gel was refilled with 100 µL pericyte cell suspension with a cell density of 1 x 10^4 cells along with 200 µL of new media. Culture plates were

incubated under humidified atmosphere of 5% CO_2 at 37°C. Basic media was replaced every 24 hours in the first two days of preparation and every other day after that. For seeding onto coverslips, cells (pericytes or MSCs purchased from Promocell GmbH (human, from bone marrow)) were seeded onto 13 mm glass coverslips at a density of 1 x 10^4 cells in 1 ml of complete media.

Cells were cultured for times indicated in the figures. Briefly, for on gel PCR 1 week was used, for metabolomics 1 and 4 weeks were used, for directed differentiation using induction media and bioactive metabolites 3 weeks was used (4 weeks for von Alizarin red).

Chondrogenic differentiation was induced using micromass culture[48, 49] and DMEM containing 10% FBS, insulin (6.25 µg/ml), dexamethasone (100 nM), ascorbate-2-phosphate (50 nM), transforming growth factor (TGF-β1, 10 ng/ml) and sodium pyruvate (110 µg/ml). Micromass cultures were performed by 'spotting' 20 µl droplets of cell suspensions into 24 well culture plates. These were then incubated for approximately 1.5 hrs to allow cell attachment. Following this, chondrogenic media was gently added to each well plate without disturbing the cells. Osteogenic differentiation was induced using complete DMEM containing 10% FBS, dexamethasone (100 nM) and ascorbate-2-phosphate (350 µM) on cells seeded as a suspension in 1 ml of media.

Cholesterol sulphate (Sigma-Aldrich) and GP18:0 (Avanti polar lipids) stock solutions were made up in DMSO and subsequently serially diluted in complete medium to final concentrations of 1 µM for cholesterol sulphate and 0.1 µM for GP18:0. Care was taken to ensure that the final DMSO concentration in any of the working solutions was less than 0.2%. Cells were maintained in culture with each of the compounds, at each concentration, for the experiment duration.

For all differentiation and metabolite test item cultures, the media was changed twice weekly for the duration the experiment

Immunofluorescence cell staining

After 3 weeks in culture (unless otherwise stated), the cells were washed once in PBS and fixed with 10% formaldehyde at 37°C for 15 min. When fixed, the samples were permeabilised using a buffer solution (10.3 g sucrose, 0.292 g NaCl, 0.06 g $MgCl_2$,

0.476 g Hepes buffer, 0.5 ml Triton X, in 100 ml water, pH 7.2) at 4°C for 5 min. The samples were then incubated at 37°C for 5 min in 1% BSA/PBS, followed by the addition of the primary antibody (1:50 in 1% BSA/PBS, monoclonal anti-human osteopontin, osteocalcin, SOX-9, nestin, myoD, β_3 tubulin and aggrecan raised in mouse (IgG1), Santa Cruz Biotechnology Inc) for 1h (37°C). Simultaneously, rhodamine conjugated phalloidin was added for the duration of this incubation (1:100 in 1% BSA/PBS, Invitrogen, UK). The samples were then washed in 0.5% Tween 20/PBS (5 min, x3). A secondary, biotin-conjugated antibody (1:50 in 1% BSA/PBS, monoclonal anti-mouse (IgG), Vector Laboratories, Peterborough, UK) was added for 1 h (37°C) followed by washing. A FITC conjugated streptavidin third layer was added (1:50 in 1% BSA/ PBS, Vector Laboratories, Peterborough, UK) at 4°C for 30 min, and given a final wash.

Samples were mounted onto a drop of DAPI (Vector Laboratories, Peterborough, UK) on a microscope slide then viewed using a fluorescence microscope (Zeiss Axiovert 200M).

Fluorescence microscopy images of cell components were overlayed using RGB stack in Image J (software v1.48, National Institute for Health, USA). Comparative analysis to quantify cell populations positively expressing gene markers and the areas relative areas with increased fluorescence intensities were also performed using threshold/contrast isolation in ImageJ to measure differences in expression level or to detect and count a cell component

Alizarin red staining

Cells maintained in culture for 3 weeks were washed with PBS and fixed with 10% formaldehyde for 20 minutes. Following this, cells were washed with sterile water and incubated with alizarin red solution (8.3 mM, pH 4.2) for 1 hr at room temperature. Cells were then washed until clear with sterile water and stored in sterile water for microscopy.

QRT-PCR analysis

For figure 1, RNA extractions from cells cultured on hydrogel biomaterials and tissue culture controls for 1, 2 or 4 week were done using the Trizol extraction reagent

(Invitrogen). For figures 3 and 4, cells cultured for 3 weeks on culture well plastic had RNA retrieved using RNeasy micro kit (Qiagen), both protocols were carried out as per manufacturers instructions. Reverse transcription to obtain cDNA was done using Quantitech reverse transcription kit (Qiagen) for all samples, also according to the manufacturers protocol.

Amplification by qRT-PCR was done using human specific primers for Glut-4, collagen type II, osteopontin, nestin, β3-tubulin and GFAP (Eurofins MWG Operon) detailed in table 1. PCR was carried out using a 7500 Real time PCR system & software (Applied Biosystems). Samples had a total reaction volume of 20 µl containing 2 µl of diluted cDNA, each reverse and forward primer at a final concentration of 100 µM and analysed using SYBR green chemistry (Qiagen). For PCR amplification samples were held at 50°C for 2 minutes then 95°C for 10 min then amplified using 95°C for 15 s and 60°C for 1 min for 40 cycles. The specificity of the PCR amplification was checked with a heat dissociation curve (measured between 60 – 95°C) done subsequent to the final PCR cycle. Gene expression levels were standardised using GAPDH as an internal control. Quantification analysis was performed using the comparative ΔΔCt method[50] and gene expression expressed as fold change relative to the control sample.

Samples were assayed in quadruplicate and gene expression was expressed as mean ± SEM.

Table 1. Real time PCR primers used to quantify mRNA expression from human genes.

Gene		
Glut-4	Forward	5'-ATG TTG CGG AGG CTA TGGG-3'
	Reverse	5'-AAA GAG AGG GTG TCC GGT GG-3'
PPAR-γ	Forward	5'-TGT GAA GCC CAT TGA AGA CA-3'
	Reverse	5'-CTG CAG TAG CTG CAC GTG TT-3'
SOX-9	Forward	5'-AGA CAG CCC CCT ATC GAC TT-3'
	Reverse	5'-CGG CAG GTA CTG GTC AAA CT-3'
Collagen type II (Col2a1)	Forward	5'-CACC TGG GAC TGT CCT CTG CGA-3'
	Reverse	5'-CCT TTG GTC CTG GTT GCC CAC T-3'
Aggrecan (ACAN)	Forward	5'-TAC ACT GGC GAG CAC TGT AAC-3'
	Reverse	5'-CAG TGG CCC TGG TAC TTG TT-3'

RUNX-2	Forward	5’-GGT CAG ATG CAG GCG GCC-3’
	Reverse	5’-TAC GTG TGG TAG CGC GTC-3’
Osteopontin (OPN)	Forward	5’-AGC TGG ATG ACC AGA GTG CT- 3’
	Reverse	5’-TGA AAT TCA TGG CTG TGG AA -3’
MyoD	Forward	5’-CAC TAC AGC GGC GAC TCC-3’
	Reverse	5’-TAG GCG CCT TCG TAG CAG-3’
Myogenin	Forward	5’-GCT CAG CTC CCT CAA CCA-3’
	Reverse	5’-GCT GTG AGA GCT GCA TTC G-3’
Nestin	Forward	5’-GTG GGA AGA TAC GGT GGA GA-3’
	Reverse	5’-ACC TGT TGT GAT TGC CCT TC-3’
β3-tubulin	Forward	5’-CAG ATG TTC GAT GCC AAG AA -3’
	Reverse	5’-GGG ATC CAC TCC ACG AAG TA-3’
GFAP	Forward	5’-GCT TCC TGG AAC AGC AAA AC-3’
	Reverse	5’-AGG TCC TGT GCC AGA TTG TC-3’
GAPDH	Forward	5’-ACC CAG AAG ACT GTG GAT GG-3’
	Reverse	5’-TTC TAG ACG GCA GGT CAG GT-3’

Metabolomic analysis

Metabolite extraction from cells cultured on hydrogels and control samples at 1 and 4 weeks were carried out on ice using ice cold chloroform:methanol:water (1:3:1,v/v). Samples were agitated on a shaker for 1 h and maintained at 4°Cfor this duration. Samples were centrifuged to sediment the debris and the supernatant transferred to clean eppendorf tubes.10 µL of the supernatant was subsequently injected on to the LC-MS system.

The LC separation was carried out using hydrophilic interaction chromatography with a ZIC-HILIC 150 mm x 4.6 mm, 5 µm column (Merck Sequant), operated by an UltiMate liquid chromatography system (Dionex, Camberley, Surrey). The LC mobile phase was run with 0.1% formic acid in water (A) and 0.08% formic acid in acetonitrile (B). The mobile phase was run at a linear gradient for 30 minutes from 20% - 80% A, maintained at 5% A for 10 minutes and then re-equilibrated to 20% A. Mass spectrometric detection was performed using an Orbitrap Exactive (Thermo Fisher Scientific, Hemel Hempstead, U.K.) within the mass range m/z 70 – 1400 in polarity switching mode.

Chromatographic peak selection and metabolite identification were done using Ideom/MzMatch excel interface[51, 52], measured peak intensities by LC-MS were normalised against protein content as measured using the Bradford assay as detailed previously[53]. Metabolite identification was done using a set of known standards to define mass and chromatographic retention times. Putative metabolites were also identified on this basis using predicted retention times as described by Creek et al[54].

SMAD Analysis

Promocell MSCs were cultured in complete media with a cell density of $1x10^4$ cells per 13 mm diameter coverslip for 3 days. Cells were then treated with CS with final concentration of 1 µM for CS and 0.1% for DMSO for 2 days. Control samples were treated with DMSO only with final concentration of 0.1% for the last 2 days cell culture. In cell Western (ICW) was carried out for the detection of pSMAD 1/5. Cells were fixed on coverslips using 4% formaldehyde fixative buffer at 37^0C for 15 mins, and then permeabilised in cold methanol at 4^0C for 5 mins. Cells were then blocked in a 1% buffer (non-fat dry milk powder in 0.1% PBST (PBS with 1% Tween 20) buffer) at room temperature for 2 hours followed by 3 x 10 mins PBST washing. Cells were then incubated with p-SMAD 1/5 (Cal No: S463/465, Cell Signalling) and SMAD 1/5 (Cal No: D5907/D462, Cell signalling) separately at 4^0C for overnight. The primary antibodies were diluted 1:100 in blocking buffer. After 3x10 mins washes with PBST buffer, cells were incubated with 1:5000 diluted infrared labelled secondary antibody IRDye 800CW (Cal No: 926-32211, LI-COR) and 1:500 diluted CellTag 700 Stain (Cal No: 926-41090, LI-COR) at room temperature for 1 hour, and followed by 3x10 mins washes with PBST. The coverslips were then dried before infrared scanning using the LI-COR Odyssey infrared imaging system.

BMP2 antagonist treatment

Human noggin protein (Sigma, UK) was dissolved in double processed tissue culture H_2O to a final concentration of 5 ng/µL. Cells were seeded onto glass coverslips in basal medium, and after allowing cells to settle down on the substrates, 10 µL noggin solution was added to half the wells to produce a final concentration 50 ng/mL. Cells were cultured in the presence of noggin for 5 days, then the medium

was replaced with fresh medium without noggin for the rest of the culture period. After 21 days, cells were fixed and stained for osteocalcin and osteopontin as described previously.

Collagen tissue mimic culture

1 ml of type I collagen (First Link, UK, from rat tail) was cast in ThinCert tissue culture inserts within 12 well plates. For each 3 mls of collagen, 0.5ml 10x DMEM, 0.5ml FCS, 2.5ml collagen and 1ml 0.1M NaOH were mixed. 0.1 M NaOH was added drop-wise until the colour changed to red. The wells flooded with complete media as the gels set. A 70 mM Fmoc hydrogel solution was prepared as has been described and 1x 10^5 pericytes per ml of hydrogel solution were added. 1 ml of the pre-gelation/cell mix was injected into the collagen gels and cultured for 28 days. Cells were fed twice weekly with complete media or cholesterol sulphate (0.1 µM concentration) supplemented media. At the end of the culture, von Kossa staining for mineralisation was used. Gels were immersed in a 5% silver nitrate solution and each side of the hydrogel was exposed to UV light for 30 minutes. The solution was removed and gels washed with deionised water before addition of 5% sodium thiosulphate for 30 minutes. Samples were next washed under running water for 10 minutes. Hydrogels were counterstained with nuclear fast red for 10 minutes, and again solution aspirated to waste and rinsed with deionised water. Samples were rinsed in 70% ethanol for 10 minutes and then maintained in 1 x PBS solution until ready to be imaged.

Statistical Analysis

Analysis of variance (ANOVA) and Bonferroni post hoc tests were performed using GraphPad prism software to compare more than two study groups. Otherwise, an unpaired, two-tailed students t-test was carried out. Statistical significance is noted where the calculated p value is less than 0.05.

Images and data available from: http://dx.doi.org/10.5525/gla.researchdata.224

Author Contributions.

Conceptualization, MJD, RVU, BP, KB and EVA. Methodology, VJ, RVU, SCJB, SR, NJ, SF, DAL, AJU, PWJMF, NTH, EVA, MJD, KB, BP, CCW. Investigation, VJ, SCJB, SR, NJ, SF, DAL, AJU, PWJMF, NTH, EVA, KB, CCW, AM. Writing – Original Draft, MJD, RVU, BP, VJ, EVA. Writing – Review and Editing, MJD, RVU, BP, VJ, SCJB, SR, NJ, SF, DAL, AJU, PWJMF, NTH, EVA, KB, CCW. Funding Acquisition, MJD, RVU, BP. Supervision, MJD, RVU, BP.

Acknowledgements.

This work was funded by BBSRC grants BB/K006908/1 and BB/J018902/1. We also acknowledge funding for EVA from the EPSRC DTC in cell and proteomic technologies. BP is funded by grants from CIRM and BHF. We acknowledge the technical assistance of Mrs Carol-Anne Smith. We acknowledge financial conflict of interest as RVU is CSO of Biogelx ltd., a spinout company that markets the gels developed in this paper.

Figure Legends.

Figure 1. *Self-assembly of two-component gelators and analysis of primary pericyte differentiations. (a) Schematic presentation of proposed core-shell nanostructures. (b) AFM images of Fmoc-F_2, Fmoc-S and the 50:50 mixture. Structures of Fmoc-F_2 and Fmoc-S are shown in supplemental Fig 1l. (c) Fluorescence emission spectra show a sharp peak at 320nm corresponding to monomeric emission of the fluorenyl moiety, with an broad peak at 460-480 nm due to the formation of aggregated excimers. The peak at 380 nm for Fmoc-S indicates the differential fluorenyl organisation upon formation of spherical aggregates (Supplemental Fig 1B). (d) FTIR spectra of Fmoc-F_2 show a band (1625-1640 cm^{-1}) due to the peptide amide I modes that are consistent with a well-ordered β-sheet-like arrangement and a second band at 1687 cm^{-1} which relates to the ordered carbamate moiety. For Fmoc-S, a carboxylate peak is evident at 1590 cm^{-1} which loses intensity and broadens in the mixture of the two components, consistent with co-assembly. (e) Oscillatory rheology of the gels show elastic moduli of different concentration gels. Results show that the stiffness increases when the concentration increases. (f) Macroscopic images for 10, 20, 40 mM gels in culture media. Pericytes were assessed for the expression of (g) β3 tubulin (neural cells), (h) SOX-9 (chondrocytes) and (i) RUNX2 (osteoblasts) on each hydrogel type with primary expression of β3 tubulin being observed on the 2 kPa (soft) surface, SOX-9 on the 15 kPa (stiff) surface and RUNX2 on the 40 kPa (rigid) surface after 1 week of culture. It is important to note that cells were only cultured in basal media*

*with no differentiation enhancing factors and so differentiation is purely substrate driven. Stats by ANOVA and Bonferroni post hoc test; control was pericytes on glass coverslips with standard media, * p < 0.05 & *** p < 0.001. Error bars = standard error from the mean; n = 4 material replicates for PCR. Note that other marker transcripts were tested for and are shown in supplemental figure 3 to confirm this analysis.*

Figure 2. *Identification of candidate metabolites with roles in lineage specific differentiation. After 1 and 4 weeks of pericyte culture on the hydrogels, whole metabolome analysis (LC-MS) was performed and from the whole metabolome, lipids were selected as a group with distinct changes where depletions were abundant. From the lipids, selected depletions for each stiffness - (a) stiff (15 kPa) and (b) rigid (40 kPa) - were identified (arrows from heatmaps to bar charts). Analysis of average peak intensities of the metabolites GP18:0 and cholesterol sulphate (CS) measured after 1 and 4 weeks in culture is illustrated as bar charts with significant depletions noted in pericytes on stiff and rigid gels respectively. Each metabolite was observed as having depletive characteristic particular to substrate stiffness, suggesting lineage-specific demand (i.e. GP 18:0 in chondrogenesis and CS in osteogenesis). When these metabolites were placed within their KEGG pathways of glycerolipid and steroid biosynthesis using stacked bar charts, the 'hit' metabolites were seen to be major depletions (each metabolite is shown at 1 week (1W) and 4 weeks (4W) of culture). Stats by ANOVA and Bonferroni post hoc test. For individual lipid plots, * p < 0.05 & *** p < 0.001. For KEGG plots, § denotes significant depletion on the stiff gel and # denotes significant depletion on the rigid gel. Error bars = standard error from the mean; n = 3 material replicates. A.u. = arbitrary units. Please note that log scale graphs are used.*

Figure 3. *Testing of biological molecule driving of osteogenesis and chondrogenesis. (a-d) For osteogenic assays, cells were cultured for 3 weeks with standard media, media containing CS or osteo-indictive media (OIM) prior to testing. (a) Pericytes and (c) MSCs were cultured in either osteogenic inductive media (OIM) or 1µM CS and demonstrated increased expression of the osteogenic markers osteopontin and osteocalcin appearing in nodule-like formations (arrows) with addition of CS similar to that of OIM. (b) For pericytes, image analysis of osteocalcin and osteopontin staining showed signifincant increase in expression for both osteoblast-related proteins with use of OIM or CS enhanced media from use of standard media alone and analysis of bone nodule area from alizarin red histology for showed nodules to be larger with CS than with OIM. (d) For MSCs, image analysis of osteopontin staining showed signifincant increase in expression for the osteoblast-related protein with use of OIM or CS enhanced media from use of standard media alone and alizarin red stain for calcium illustrated appearance of bone nodules appearing in MSCs cultures treated with CS (arrows). For chondrogenic assays (e-h), cells were maintained using micromass culture for 10 days without/without the addition of 0.1 µm GP18:0 or chondro-inductive media (CIM) prior to testing. Collagen II (Col II – pericyte) or SOX9 (MSC) and aggrecan (ACAN) expression was noted in pericyte (e) and MSC (g) cultures with either chondro-inductive media (CIM) or GP18:0 but not on control coverslips with basal media (arrows). Image analysis showed significantly*

*increased expression of both aggrecan and collagen II with addition of CIM and GP18:0 with pericytes (f) and increased expression of SOX9 and aggrecan with MSCs (h). Error bars = standard deviations. For PCR n=4 replicates, for image analysis data is obtained from >120 cells from 4 replicates. Stats by ANOVA followed and Bonferroni post-hoc test; * $p < 0.05$ & ** $p < 0.01$. Control was pericytes/MSCs on glass coverslips with standard media. Fluorescence images show actin cytoskeleton (red), cell nuclei (blue) and SOX9, collagen II, aggrecan, osteocalcin or osteopontin (green). A.u. = arbitrary units. Note that PCR analysis of the marker transcripts is shown in supplemental figure 10 to validate the protein data in this figure.*

Figure 4. *Testing of cholesterol sulphate mechanism. (a) Layering metabolomics data with canonical biochemical pathways using Ingenuity pathway analysis showed CS interacting with TGFβ linked to BMP signalling. (b) Testing SMAD 1 & 5 activation (phosphortylation) by in cell Western analysis after 5 days of culture on glass coverslips showed significant up-regulation of SMAD phosphorylation with addition of CS compared to use of standard media and addition of noggin (CSn) prevented CS inducement of osteocalcin and osteopontin transcripts after 21 day culture as shown by qPCR. (c) Use of the 40 kPa hydrogel loaded with pericytes injected into a collagen tissue mimic produced a degree of mineralisation within the gels after 28 days of culture as shown by von Kossa histology. However, addition of CS produced consistent, high levels of mineralisation within the gels indicating the potential of biomaterials/bioactive metabolite strategies (note the small images are similarly contrast enhanced so that the difference between non mineralised and mineralised areas are clear). For metabolomics and quantitative analysis, n=3 material replicates, stats by ANOVA followed and Bonferroni post-hoc test; * $p < 0.05$.*

References:

1. McMurray, R. J., Gadegaard, N., Tsimbouri, P. M., Burgess, K. V., McNamara, L. E., Tare, R., Murawski, K., Kingham, E., Oreffo, R. O. C., Dalby, M. J. (2011). Nanoscale surfaces for the long-term maintenance of mesenchymal stem cell phenotype and multipotency. Nat Mater**,** *10*, 637-644.
2. Yanes, O., Clark, J., Wong, D. M., Patti, G. J., Sanchez-Ruiz, A., Benton, H. P., Trauger, S. A., Desponts, C., Ding, S., Siuzdak, G. (2010). Metabolic oxidation regulates embryonic stem cell differentiation. Nature Chemical Biology**,** *6*, 411-417.
3. Tsimbouri, P. M., McMurray, R. J., Burgess, K. V., Alakpa, E. V., Reynolds, P. M., Murawski, K., Kingham, E., Oreffo, R. O., Gadegaard, N., Dalby, M. J. (2012). Using nanotopography and metabolomics to identify biochemical effectors of multipotency. ACS Nano**,** *6*, 10239-49.
4. Reyes, J. M., Fermanian, S., Yang, F., Zhou, S. Y., Herretes, S., Murphy, D. B., Elisseeff, J. H., Chuck, R. S. (2006). Metabolic changes in mesenchymal stem cells in osteogenic medium measured by autofluorescence spectroscopy. Stem Cells**,** *24*, 1213-7.
5. Haldar, M., Kohyama, M., So, A. Y., Kc, W., Wu, X., Briseno, C. G., Satpathy, A. T., Kretzer, N. M., Arase, H., Rajasekaran, N. S., et al. (2014). Heme-mediated

SPI-C induction promotes monocyte differentiation into iron-recycling macrophages. Cell**,** *156*, 1223-34.
6. Zhang, S. (2003). Fabrication of novel biomaterials through molecular self-assembly. Nat Biotechnol**,** *21*, 1171-8.
7. Aida, T., Meijer, E. W., Stupp, S. I. (2012). Functional supramolecular polymers. Science**,** *335*, 813-7.
8. Banwell, E. F., Abelardo, E. S., Adams, D. J., Birchall, M. A., Corrigan, A., Donald, A. M., Kirkland, M., Serpell, L. C., Butler, M. F., Woolfson, D. N. (2009). Rational design and application of responsive alpha-helical peptide hydrogels. Nat Mater**,** *8*, 596-600.
9. Webber, M. J., Appel, E. A., Meijer, E. W., Langer, R. (2016). Supramolecular biomaterials. Nature Materials**,** *15*, 13-26.
10. McMurray, R. J., Gadegaard, N., Tsimbouri, P. M., Burgess, K. V., McNamara, L. E., Tare, R., Murawski, K., Kingham, E., Oreffo, R. O., Dalby, M. J. (2011). Nanoscale surfaces for the long-term maintenance of mesenchymal stem cell phenotype and multipotency. Nat Mater**,** *10*, 637-44.
11. Curran, J. M., Stokes, R., Irvine, E., Graham, D., Amro, N. A., Sanedrin, R. G., Jamil, H., Hunt, J. A. (2010). Introducing dip pen nanolithography as a tool for controlling stem cell behaviour: unlocking the potential of the next generation of smart materials in regenerative medicine. Lab Chip**,** *10*, 1662-70.
12. Gilbert, P. M., Havenstrite, K. L., Magnusson, K. E., Sacco, A., Leonardi, N. A., Kraft, P., Nguyen, N. K., Thrun, S., Lutolf, M. P., Blau, H. M. (2010). Substrate elasticity regulates skeletal muscle stem cell self-renewal in culture. Science**,** *329*, 1078-81.
13. Engler, A. J., Sen, S., Sweeney, H. L., Discher, D. E. (2006). Matrix elasticity directs stem cell lineage specification. Cell**,** *126*, 677-89.
14. Benoit, D. S., Schwartz, M. P., Durney, A. R., Anseth, K. S. (2008). Small functional groups for controlled differentiation of hydrogel-encapsulated human mesenchymal stem cells. Nat Mater**,** *7*, 816-23.
15. Curran, J. M., Chen, R., Hunt, J. A. (2006). The guidance of human mesenchymal stem cell differentiation in vitro by controlled modifications to the cell substrate. Biomaterials**,** *27*, 4783-93.
16. McBeath, R., Pirone, D. M., Nelson, C. M., Bhadriraju, K., Chen, C. S. (2004). Cell shape, cytoskeletal tension, and RhoA regulate stem cell lineage commitment. Dev Cell**,** *6*, 483-95.
17. Kilian, K. A., Bugarija, B., Lahn, B. T., Mrksich, M. (2010). Geometric cues for directing the differentiation of mesenchymal stem cells. Proc Natl Acad Sci U S A**,** *107*, 4872-7.
18. Gilbert, P. M., Havenstrite, K. L., Magnusson, K. E. G., Sacco, A., Leonardi, N. A., Kraft, P., Nguyen, N. K., Thrun, S., Lutolf, M. P., Blau, H. M. (2010). Substrate Elasticity Regulates Skeletal Muscle Stem Cell Self-Renewal in Culture. Science**,** *329*, 1078-1081.
19. Trappmann, B., Gautrot, J. E., Connelly, J. T., Strange, D. G., Li, Y., Oyen, M. L., Cohen Stuart, M. A., Boehm, H., Li, B., Vogel, V., et al. (2012). Extracellular-matrix tethering regulates stem-cell fate. Nat Mater**,** *11*, 642-9.

20. Gobaa, S., Hoehnel, S., Roccio, M., Negro, A., Kobel, S., Lutolf, M. P. (2011). Artificial niche microarrays for probing single stem cell fate in high throughput. Nat Methods**,** *8*, 949-55.
21. Swift, J., Ivanovska, I. L., Buxboim, A., Harada, T., Dingal, P. C., Pinter, J., Pajerowski, J. D., Spinler, K. R., Shin, J. W., Tewari, M., et al. (2013). Nuclear lamin-A scales with tissue stiffness and enhances matrix-directed differentiation. Science**,** *341*, 1240104.
22. Lutolf, M. P., Hubbell, J. A. (2005). Synthetic biomaterials as instructive extracellular microenvironments for morphogenesis in tissue engineering. Nat Biotechnol**,** *23*, 47-55.
23. Anderson, D. G., Levenberg, S., Langer, R. (2004). Nanoliter-scale synthesis of arrayed biomaterials and application to human embryonic stem cells. Nat Biotechnol**,** *22*, 863-6.
24. Jayawarna, V., Richardson, S. M., Hirst, A. R., Hodson, N. W., Saiani, A., Gough, J. E., Ulijn, R. V. (2009). Introducing chemical functionality in Fmoc-peptide gels for cell culture. Acta Biomater**,** *5*, 934-43.
25. Collier, J. H., Rudra, J. S., Gasiorowski, J. Z., Jung, J. P. (2010). Multi-component extracellular matrices based on peptide self-assembly. Chem Soc Rev**,** *39*, 3413-24.
26. Shi, J., Gao, Y., Zhang, Y., Pan, Y., Xu, B. (2011). Calcium ions to cross-link supramolecular nanofibers to tune the elasticity of hydrogels over orders of magnitude. Langmuir**,** *27*, 14425-31.
27. Pashuck, E. T., Cui, H., Stupp, S. I. (2010). Tuning supramolecular rigidity of peptide fibers through molecular structure. J Am Chem Soc**,** *132*, 6041-6.
28. Silva, G. A., Czeisler, C., Niece, K. L., Beniash, E., Harrington, D. A., Kessler, J. A., Stupp, S. I. (2004). Selective differentiation of neural progenitor cells by high-epitope density nanofibers. Science**,** *303*, 1352-5.
29. Dankers, P. Y. W., Harmsen, M. C., Brouwer, L. A., Van Luyn, M. J. A., Meijer, E. W. (2005). A modular and supramolecular approach to bioactive scaffolds for tissue engineering. Nat Mater**,** *4*, 568-574.
30. Zhou, M., Smith, A. M., Das, A. K., Hodson, N. W., Collins, R. F., Ulijn, R. V., Gough, J. E. (2009). Self-assembled peptide-based hydrogels as scaffolds for anchorage-dependent cells. Biomaterials**,** *30*, 2523-30.
31. Fleming, S., Debnath, S., Frederix, P. W., Hunt, N. T., Ulijn, R. V. (2014). Insights into the Coassembly of Hydrogelators and Surfactants Based on Aromatic Peptide Amphiphiles. Biomacromolecules.
32. Jayawarna, V., Ali, M., Jowitt, T. A., Miller, A. E., Saiani, A., Gough, J. E., Ulijn, R. V. (2006). Nanostructured hydrogels for three-dimensional cell culture through self-assembly of fluorenylmethoxycarbonyl-dipeptides. Advanced Materials**,** *18*, 611-+.
33. Mahler, A., Reches, M., Rechter, M., Cohen, S., Gazit, E. (2006). Rigid, self-assembled hydrogel composed of a modified aromatic dipeptide. Advanced Materials**,** *18*, 1365-+.
34. Discher, D. E., Mooney, D. J., Zandstra, P. W. (2009). Growth factors, matrices, and forces combine and control stem cells. Science**,** *324*, 1673-7.

35. Hahn, S., Kim, S. S., Lee, C., Cho, M. (2005). Characteristic two-dimensional IR spectroscopic features of antiparallel and parallel beta-sheet polypeptides: simulation studies. J Chem Phys**,** *123*, 084905.
36. Crisan, M., Yap, S., Casteilla, L., Chen, C. W., Corselli, M., Park, T. S., Andriolo, G., Sun, B., Zheng, B., Zhang, L., et al. (2008). A perivascular origin for mesenchymal stem cells in multiple human organs. Cell Stem Cell**,** *3*, 301-13.
37. Nguyen, B. V., Wang, Q. G., Kuiper, N. J., El Haj, A. J., Thomas, C. R., Zhang, Z. (2010). Biomechanical properties of single chondrocytes and chondrons determined by micromanipulation and finite-element modelling. J R Soc Interface**,** *7*, 1723-33.
38. Kim, M. K., Lee, H. Y., Park, K. S., Shin, E. H., Jo, S. H., Yun, J., Lee, S. W., Yoo, Y. H., Lee, Y. S., Baek, S. H., et al. (2005). Lysophosphatidic acid stimulates cell proliferation in rat chondrocytes. Biochemical Pharmacology**,** *70*, 1764-1771.
39. Itoh, R., Miura, S., Takimoto, A., Kondo, S., Sano, H., Hiraki, Y. (2010). Stimulatory actions of lysophosphatidic acid on mouse ATDC5 chondroprogenitor cells. J Bone Miner Metab**,** *28*, 659-71.
40. Hurst-Kennedy, J., Boyan, B. D., Schwartz, Z. (2009). Lysophosphatidic acid signaling promotes proliferation, differentiation, and cell survival in rat growth plate chondrocytes. Biochim Biophys Acta**,** *1793*, 836-46.
41. Strott, C. A., Higashi, Y. (2003). Cholesterol sulfate in human physiology: what's it all about? Journal of Lipid Research**,** *44*, 1268-1278.
42. Woscholski, R., Kodaki, T., Palmer, R. H., Waterfield, M. D., Parker, P. J. (1995). Modulation of the substrate-specificity of the mammalian phosphatidylinositol 3-kinase by cholesterol sulfate and sulfatide. Biochemistry**,** *34*, 11489-11493.
43. Iwata, J.-i., Hosokawa, R., Sanchez-Lara, P. A., Urata, M., Slavkin, H., Chai, Y. (2010). Transforming Growth Factor-beta Regulates Basal Transcriptional Regulatory Machinery to Control Cell Proliferation and Differentiation in Cranial Neural Crest-derived Osteoprogenitor Cells. Journal of Biological Chemistry**,** *285*, 4975-4982.
44. Nawaz, S. Z., Bentley, G., Briggs, T. W., Carrington, R. W., Skinner, J. A., Gallagher, K. R., Dhinsa, B. S. (2014). Autologous chondrocyte implantation in the knee: mid-term to long-term results. J Bone Joint Surg Am**,** *96*, 824-30.
45. Bourassa, P., Dubeau, S., Maharvi, G. M., Fauq, A. H., Thomas, T. J., Tajmir-Riahi, H. A. (2011). Locating the binding sites of anticancer tamoxifen and its metabolites 4-hydroxytamoxifen and endoxifen on bovine serum albumin. Eur J Med Chem**,** *46*, 4344-53.
46. Javid, N., Roy, S., Zelzer, M., Yang, Z., Sefcik, J., Ulijn, R. V. (2013). Cooperative self-assembly of peptide gelators and proteins. Biomacromolecules**,** *14*, 4368-76.
47. Corselli, M., Crisan, M., Murray, I. R., West, C. C., Scholes, J., Codrea, F., Khan, N., Peault, B. (2013). Identification of perivascular mesenchymal stromal/stem cells by flow cytometry. Cytometry. Part A : the journal of the International Society for Analytical Cytology**,** *83*, 714-20.
48. Chonanant, C., Bambery, K. R., Jearanaikoon, N., Chio-Srichan, S., Limpaiboon, T., Tobin, M. J., Heraud, P., Jearanaikoon, P. (2014). Discrimination of micromass-induced chondrocytes from human mesenchymal stem cells by

focal plane array-Fourier transform infrared microspectroscopy. Talanta**,** *130*, 39-48.
49. Mello, M. A., Tuan, R. S. (1999). High density micromass cultures of embryonic limb bud mesenchymal cells: An in vitro model of endochondral skeletal development. In Vitro Cellular & Developmental Biology-Animal**,** *35*, 262-269.
50. Schefe, J. H., Lehmann, K. E., Buschmann, I. R., Unger, T., Funke-Kaiser, H. (2006). Quantitative real-time RT-PCR data analysis: current concepts and the novel "gene expression's C-T difference" formula. Journal of Molecular Medicine-Jmm**,** *84*.
51. Creek, D. J., Jankevics, A., Burgess, K. E., Breitling, R., Barrett, M. P. (2012). IDEOM: an Excel interface for analysis of LC-MS-based metabolomics data. Bioinformatics**,** *28*, 1048-9.
52. Scheltema, R. A., Jankevics, A., Jansen, R. C., Swertz, M. A., Breitling, R. (2011). PeakML/mzMatch: a file format, Java library, R library, and tool-chain for mass spectrometry data analysis. Anal Chem**,** *83*, 2786-93.
53. Compton, S. J., Jones, C. G. (1985). Mechanism of dye response and interference in the bradford protein assay. Analytical Biochemistry**,** *151*.
54. Creek, D. J., Jankevics, A., Breitling, R., Watson, D. G., Barrett, M. P., Burgess, K. E. (2011). Toward global metabolomics analysis with hydrophilic interaction liquid chromatography-mass spectrometry: improved metabolite identification by retention time prediction. Anal Chem**,** *83*, 8703-10.

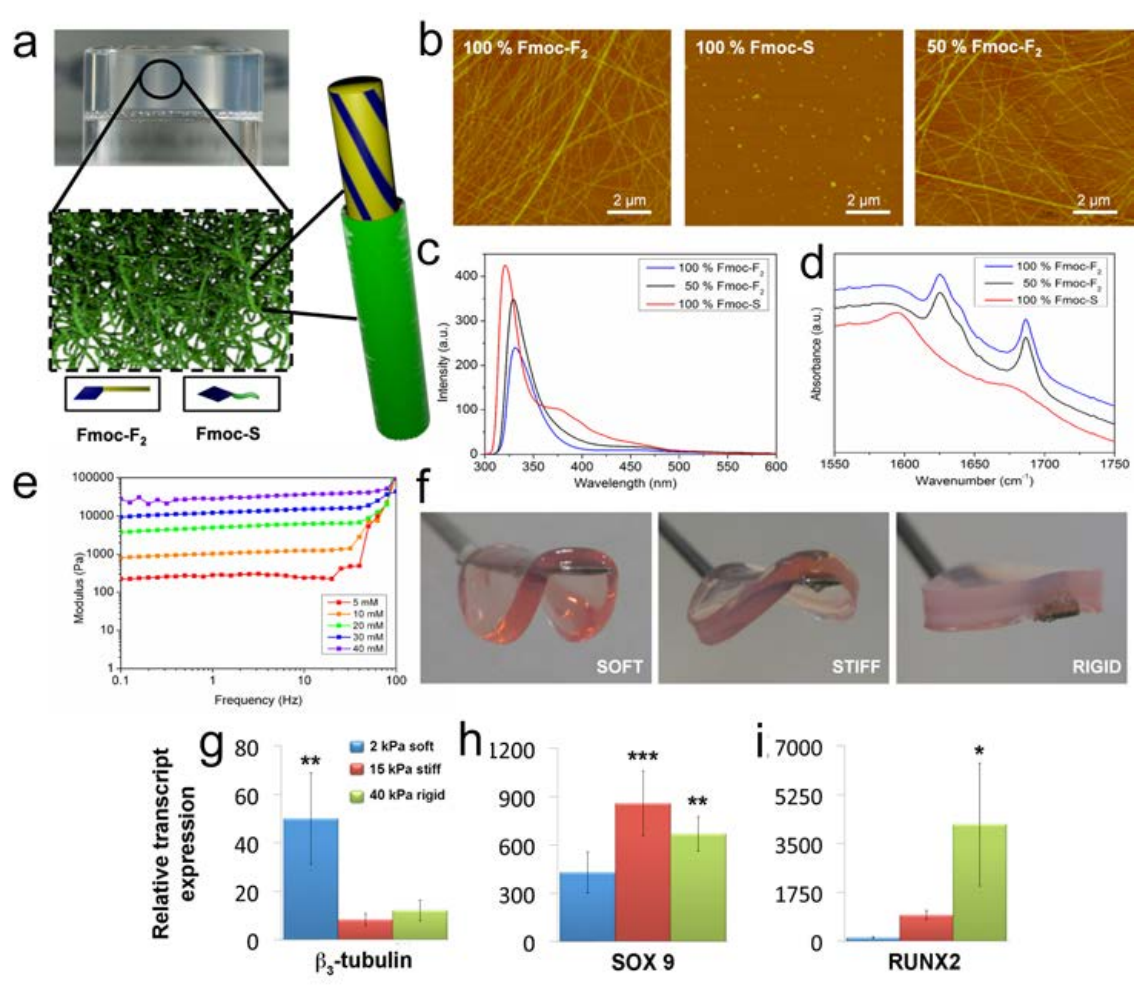
a
Fmoc-F2
Fmoc-S
b
100 % Fmoc-F2
100 % Fmoc-S
50 % Fmoc-F2
2 µm
2 µm
2 µm
c
100 % Fmoc-F2
50 % Fmoc-F2
100 % Fmoc-S
Intensity (a.u.)
Wavelength (nm)
d
100 % Fmoc-F2
50 % Fmoc-F2
100 % Fmoc-S
Absorbance (a.u.)
Wavenumber (cm-1)
e
Modulus (Pa)
Frequency (Hz)
5 mM
10 mM
20 mM
30 mM
40 mM
f
SOFT
STIFF
RIGID
g
Relative transcript expression
2 kPa soft
15 kPa stiff
40 kPa rigid
β3-tubulin
h
SOX 9
i
RUNX2

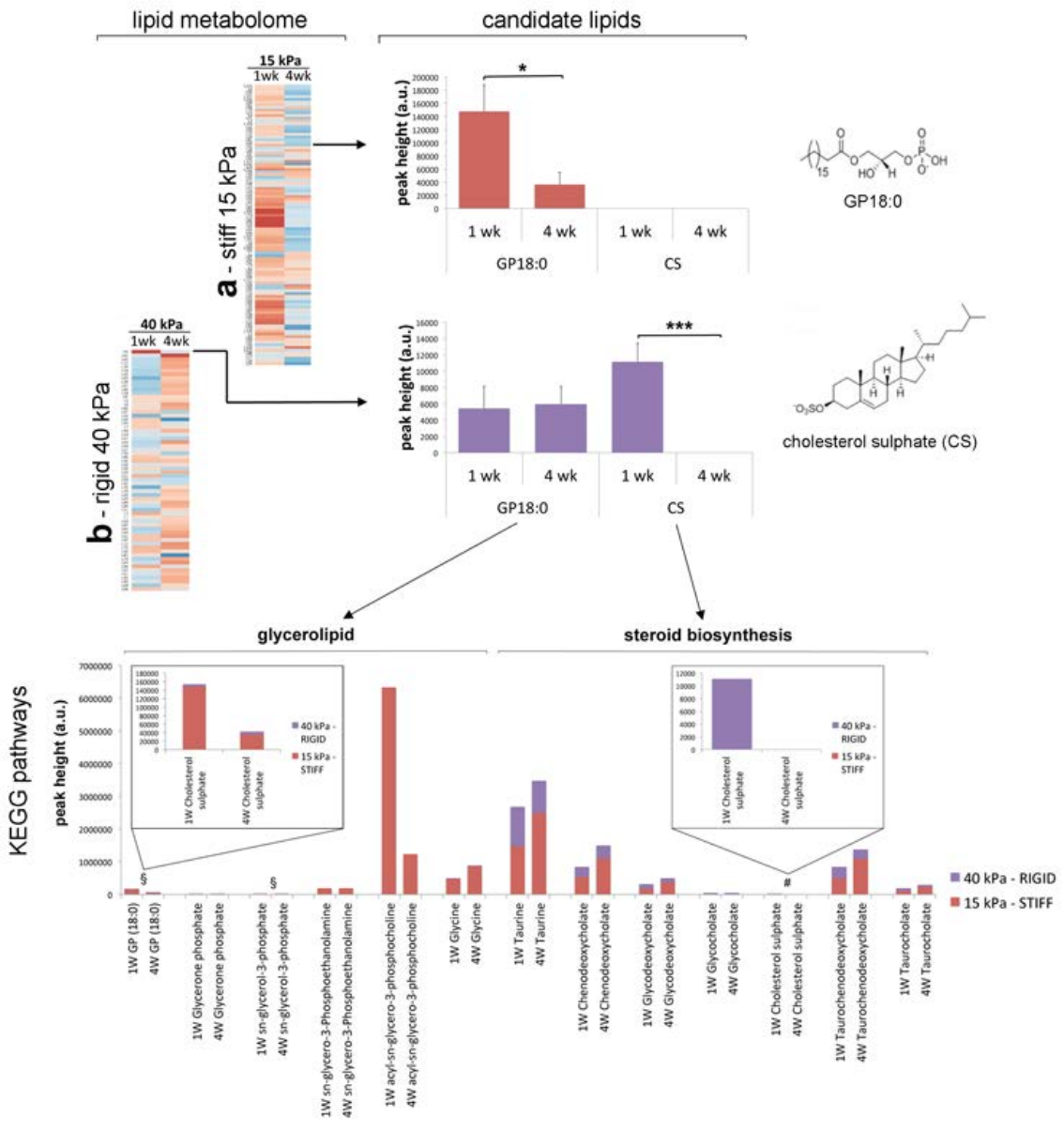
lipid metabolome
candidate lipids
15 kPa
1wk 4wk
a - stiff 15 kPa
peak height (a.u.)
*
1 wk
4 wk
GP18:0
CS
GP18:0
40 kPa
1wk 4wk
b - rigid 40 kPa
***
cholesterol sulphate (CS)
glycerolipid
steroid biosynthesis
KEGG pathways
40 kPa - RIGID
15 kPa - STIFF
1W GP (18:0)
4W GP (18:0)
1W Glycerone phosphate
4W Glycerone phosphate
1W sn-glycerol-3-phosphate
4W sn-glycerol-3-phosphate
1W sn-glycero-3-Phosphoethanolamine
4W sn-glycero-3-Phosphoethanolamine
1W acyl-sn-glycero-3-phosphocholine
4W acyl-sn-glycero-3-phosphocholine
1W Glycine
4W Glycine
1W Taurine
4W Taurine
1W Chenodeoxycholate
4W Chenodeoxycholate
1W Glycodeoxycholate
4W Glycodeoxycholate
1W Glycocholate
4W Glycocholate
1W Cholesterol sulphate
4W Cholesterol sulphate
1W Taurochenodeoxycholate
4W Taurochenodeoxycholate
1W Taurocholate
4W Taurocholate

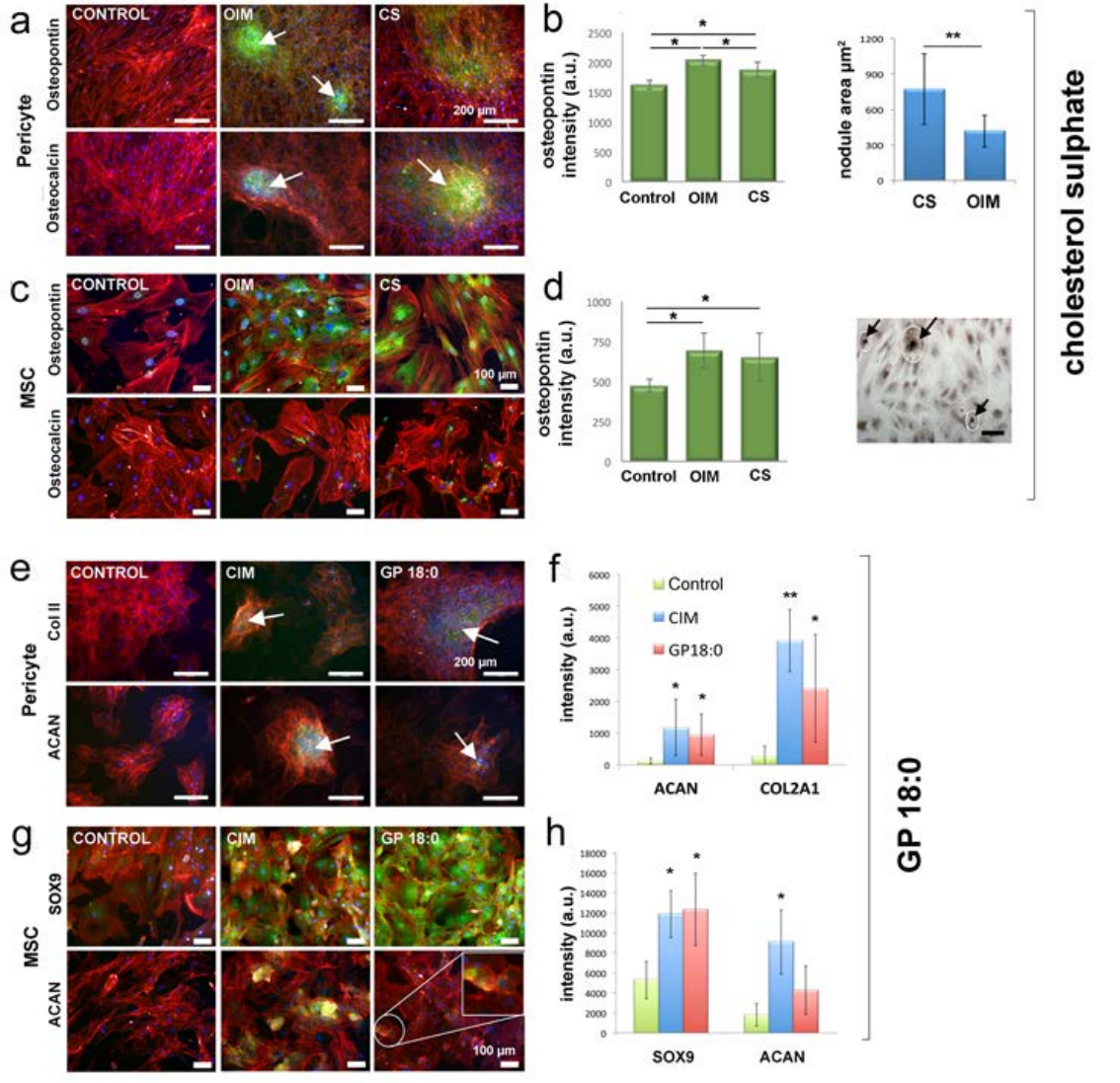
a
CONTROL
OIM
CS
Pericyte
Osteopontin
Osteocalcin
200 µm
b
osteopontin intensity (a.u.)
Control
OIM
CS
nodule area µm²
CS
OIM
cholesterol sulphate
c
CONTROL
OIM
CS
MSC
Osteopontin
Osteocalcin
100 µm
d
osteopontin intensity (a.u.)
Control
OIM
CS
e
CONTROL
CIM
GP 18:0
Pericyte
Col II
ACAN
200 µm
f
Control
CIM
GP18:0
intensity (a.u.)
ACAN
COL2A1
GP 18:0
g
CONTROL
CIM
GP 18:0
MSC
SOX9
ACAN
100 µm
h
intensity (a.u.)
SOX9
ACAN

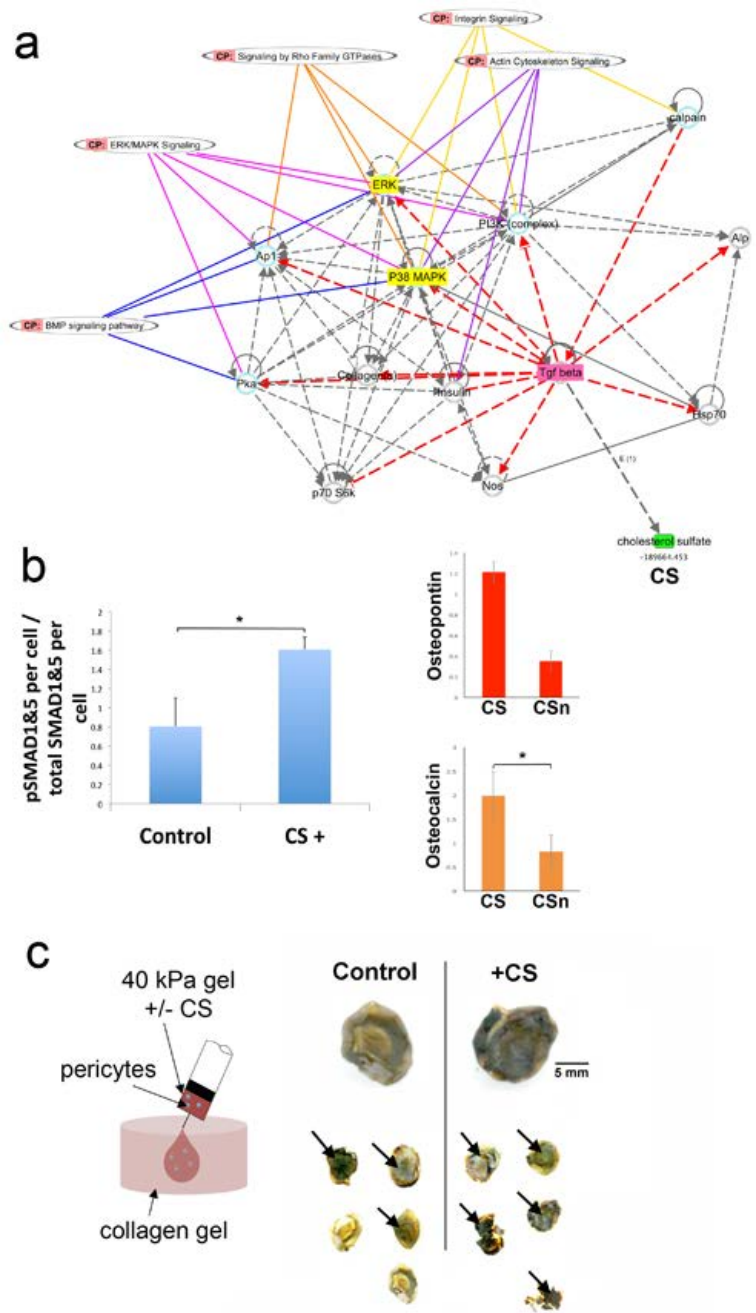
a
CP: Integrin Signaling
CP: Signaling by Rho Family GTPases
CP: Actin Cytoskeleton Signaling
calpain
CP: ERK/MAPK Signaling
ERK
PI3K (complex)
Ap1
P38 MAPK
Alp
CP: BMP signaling pathway
Pxn
Collagen()
Insulin
Tgf beta
Hsp70
p70 S6k
Nos
cholesterol sulfate
-18966.453
CS
b
pSMAD1&5 per cell / total SMAD1&5 per cell
*
Control
CS +
Osteopontin
CS
CSn
Osteocalcin
*
CS
CSn
c
40 kPa gel
+/- CS
pericytes
collagen gel
Control
+CS
5 mm